ChemPubSoc Europe

DOI: 10.1002/chem.201500556

CHEMISTRY
A European Journal
Full Paper

Molecular Probes

Distinct Spacing Between Anionic Groups: An Essential Chemical Determinant for Achieving Thiophene-Based Ligands to Distinguish β-Amyloid or Tau Polymorphic Aggregates

Therése Klingstedt,[a] Hamid Shirani,[a] Jasmin Mahler,[b, d] Bettina M. Wegenast-Braun,[b, d] Sofie Nyström,[a] Michel Goedert,[c] Mathias Jucker,[b, d] and K. Peter R. Nilsson*[a]

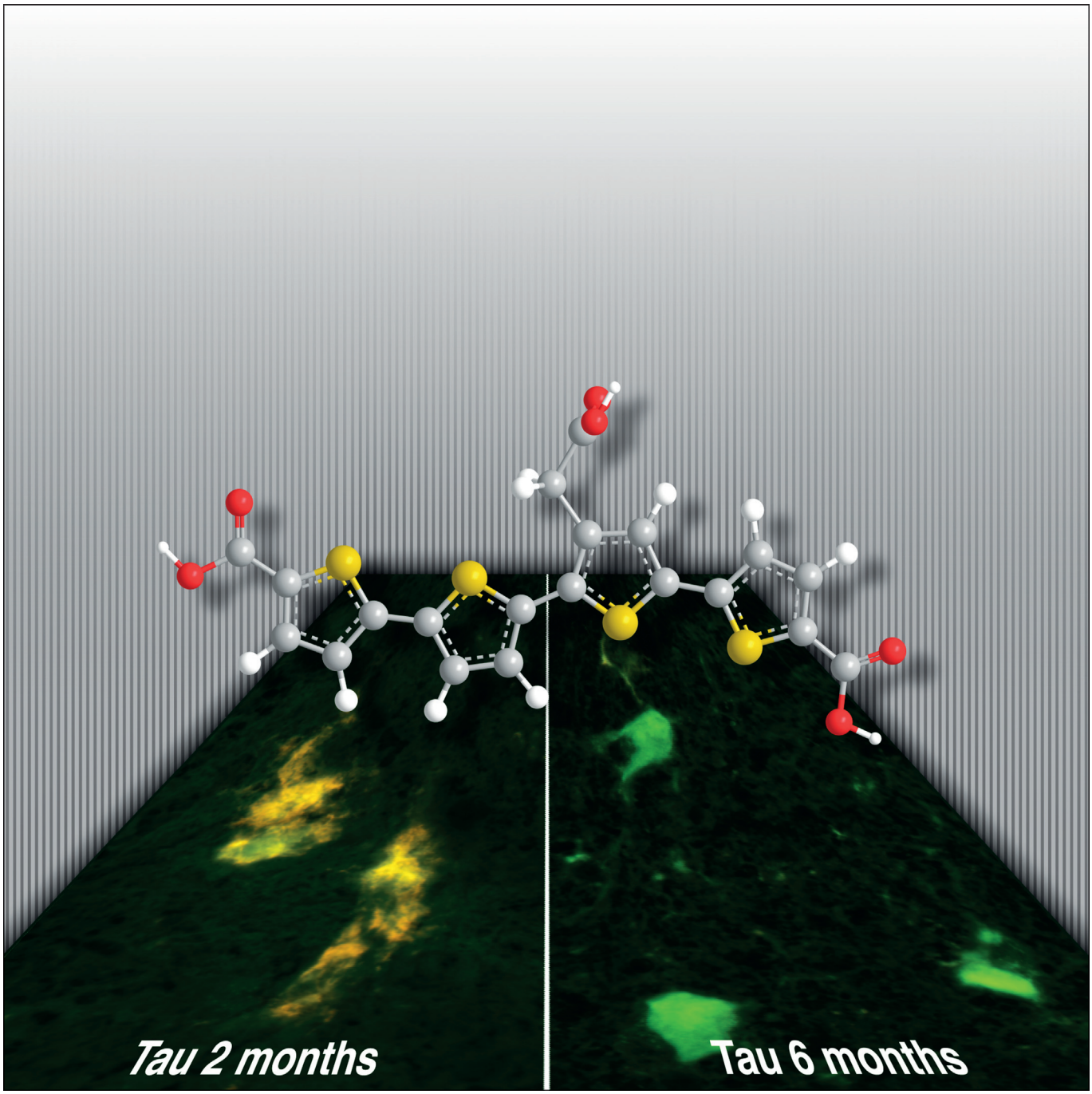

Abstract: The accumulation of protein aggregates is associated with many devastating neurodegenerative diseases and the existence of distinct aggregated morphotypes has been suggested to explain the heterogeneous phenotype reported for these diseases. Thus, the development of molecular probes able to distinguish such morphotypes is essential. We report an anionic tetrameric oligothiophene compound that can be utilized for spectral assignment of different morphotypes of β-amyloid or tau aggregates present in transgenic mice at distinct ages. The ability of the ligand to spectrally distinguish between the aggregated morphotypes was reduced when the spacing between the anionic substituents along the conjugated thiophene backbone was altered, which verified that specific molecular interactions between the ligand and the protein aggregate are necessary to detect aggregate polymorphism. Our findings provide the structural and functional basis for the development of new fluorescent ligands that can distinguish between different morphotypes of protein aggregates.

Introduction

The accumulation of protein aggregates in various organs is the pathognomonic feature of several human diseases and great effort has been devoted to unravel the association between protein deposition and pathogenesis.[1] In the aggregated structures, the protein polypeptide chain is arranged in a highly regular manner[2,3] and small hydrophobic ligands with an affinity for this structural regularity have been developed.[4] For many years, congo red and thioflavin T (ThT) have been the standard choices for detection of protein aggregates, or amyloid, and their structures have been subjected to various modifications to enhance their performance as amyloid ligands.[4–6] However, these conventional dyes cannot be used to distinguish and study different morphotypes of protein aggregates, a phenomenon reported for an increasing number of proteins associated with neurodegenerative diseases.[7–12]

The prion protein is a classic example of how an identical primary sequence of amino acids can misfold into distinct aggregate morphotypes, which gives rise to specific prion strains.[13] Similar polymorphism has also been suggested for the β-amyloid (Aβ) peptide, one of the histopathological hallmarks of Alzheimer's disease (AD), because variations in Aβ aggregate morphology can be seen in both AD patients[14] and in AD transgenic-mouse models.[15] Seeding experiments in vitro[16] and in mice[15] have shown that the structure of the seed used is self-propagated to the newly formed fibrils, and it was recently demonstrated that seeding with Aβ aggregates extracted from two AD patients with distinct clinical history and pathology resulted in fibrils with two different structures.[17] In addition, a conformational variation of α-synuclein aggregates in patients with Parkinson's disease (PD)[12] and the presence of distinct aggregated tau conformers in human tauopathies[11,18] have been suggested. Hence, the existence of distinct aggregate morphotypes has been suggested to explain the heterogeneous phenotype reported for several neurodegenerative protein-aggregation diseases, and the development of molecular probes able to detect and distinguish heterogenic protein deposits is highly important.

Luminescent conjugated oligo- and polythiophenes (LCOs and LCPs) are optical amyloid ligands that have been utilized for spectral discrimination between polymorphic protein aggregates.[19] Distinct conformational restrictions of the conjugated thiophene backbone result in different colors being emitted from the probe and this conformationally induced optical phenomenon has been utilized to discriminate prion-strain-specific protein aggregates,[20,21] protein deposits found in different types of systemic amyloidosis,[22] and polymorphic Aβ aggregates.[23,24] Recently, it was also shown that a combination of LCOs can be used to monitor age-related structural rearrangements of Aβ deposits in transgenic mice.[25]

LCOs with distinct chemical compositions can also be employed for spectral separation of Aβ and tau aggregates, the two major histopathological hallmarks of AD.[26–29] In human brain tissue samples with AD pathology, the anionic tetrameric LCO HS-68 (Figure 1 A) was reported to demonstrate a wide distribution in emission spectra within the populations of Aβ deposits and tau aggregates.[29] Herein, HS-68 was applied to brain-tissue sections from transgenic mice with Aβ or tau pathology and the variation in the emission profiles from HS-68 could be assigned to age-dependent polymorphism of the Aβ deposits and tau aggregates. In addition, subtle changes to the chemical composition of HS-68 were shown to reduce or eliminate its capacity for spectral identification of the distinct aggregate morphologies of Aβ and tau. Thus, these findings might aid the chemical design of optimal ligands for recognizing and studying different morphotypes of protein aggregates.

[a] *Dr. T. Klingstedt, Dr. H. Shirani, Dr. S. Nyström, Dr. K. P. R. Nilsson*
Department of Chemistry, Linköping University
SE-581 83 Linköping (Sweden)
E-mail: petni@ifm.liu.se

[b] *J. Mahler, Dr. B. M. Wegenast-Braun, Prof. M. Jucker*
Department of Cellular Neurology
Hertie Institute for Clinical Brain Research
University of Tübingen, Tübingen (Germany)

[c] *Dr. M. Goedert*
MRC Laboratory of Molecular Biology, Cambridge (United Kingdom)

[d] *J. Mahler, Dr. B. M. Wegenast-Braun, Prof. M. Jucker*
DZNE, German Center for Neurodegenerative Diseases, Tübingen (Germany)

Supporting information for this article is available on the WWW under http://dx.doi.org/10.1002/chem.201500556. This contains full experimental details, including additional characterization data and NMR spectra of new compounds.

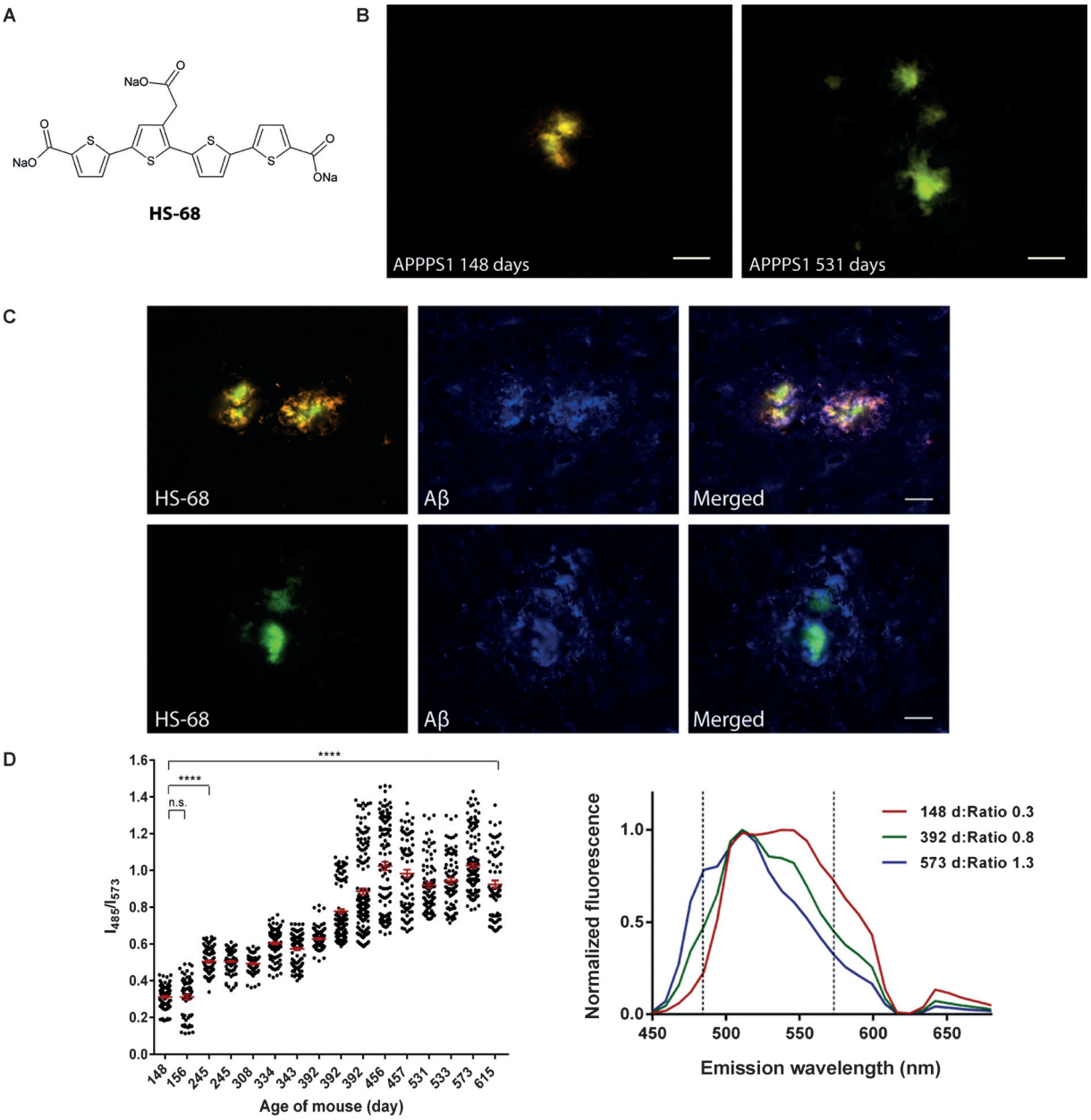

Figure 1. Chemical structure, fluorescence images, and emission analysis of HS-68 upon binding to Aβ deposits. A) The chemical structure of the sodium salt HS-68. B) Fluorescence images of Aβ deposits in frozen brain sections from APPPS1 mice sacrificed at 148 or 531 d labeled with HS-68. The sections were fixed with ethanol before staining with HS-68 (3 μM) in phosphate-buffered saline at pH 7.4. The probe displays a blueshift in color for old versus young mice. Scale bar = 20 μm. C) Fluorescence images showing colabeling of an anti-Aβ antibody (6E10) and HS-68 in acetone-fixed frozen brain sections from one young (top) and one old (bottom) APPPS1 mouse. Scale bar = 20 μm. D) Plot of the ratio of the fluorescence intensity at $\lambda = 485$ and 573 nm in the HS-68 emission spectra (excited at $\lambda = 405$ nm) collected from the central core of Aβ deposits in ethanol-fixed frozen brain sections from APPPS1 mice (left). As the mice ages the ratio increases, which confirms the blueshift in HS-68 emission upon aging. The group mean and standard error of the mean are indicated. Data were analyzed by one-way analysis of variance followed by Tukey's multicomparison post hoc test. **** = $p < 0.0001$, n.s. = non-significant. In the spectral graph, representative emission spectra of HS-68 bound to an Aβ plaque in APPPS1 mice sacrificed at 148, 392, or 573 d. Dashed lines (-----) indicate selected emission wavelengths when generating the ratio plot.

Results and Discussion

Age-dependent emission profiles of HS-68

HS-68 (Figure 1 A) was reported to display a broad variation in emission spectra when bound to Aβ deposits, as well as to tau aggregates, in human AD brain-tissue sections,[29] therefore the probe was applied to brain-tissue sections from transgenic mice with Aβ (APPPS1 mice) or tau (P301S tau mice) pathology. Cohorts of transgenic mice with a broad age span were analyzed, since age-related differences for Aβ deposits and morphological variants of tau aggregates have been reported for these mouse models.[25,30] In APPPS1 mice, HS-68 strongly labeled the Aβ deposits and different types of aggregates could be distinguished, both by their morphological appearance[31]

and by distinct HS-68 fluorescence. For small and dense deposits, mainly found in young animals, HS-68 staining resulted in a yellowish color from the compact core and a red color from the fibrilar tentacles protruding from the center (Figure 1B; Supporting Information, Figure S1). In older mice the plaques were larger and HS-68 emission was markedly blueshifted when binding to the cores and the surrounding diffuse amyloid structures, rendering green-colored deposits (Figure 1B). Colocalization between HS-68 and an antibody against Aβ confirmed that HS-68 positive deposits in both young and old animals were composed of Aβ (Figure 1C). Spectral analysis of the compact core of Aβ aggregates in mice sacrificed at different ages verified the variation in HS-68 emission characteristics as the mice aged (Figure 1D; Supporting Information, Figure S1). Representative spectra for deposits in mice sacrificed at 148, 392, or 573 d all displayed emission peaks at $\lambda =$ 511 nm, but with additional pronounced shoulders at $\lambda \approx 570$ nm for the youngest mice and $\lambda \approx 485$ nm for the oldest mice, which confirmed red- and blueshifted HS-68 emission characteristics, respectively (Figure 1D). By plotting the ratio of the fluorescence intensity at $\lambda = 485$ and 573 nm as an indicator for the HS-68 emission profile, it was clearly shown that young mice mostly displayed Aβ aggregates with a redshifted HS-68 spectrum, whereas a broader distribution of the HS-68 spectra was observed for older mice (>392 d; Figure 1D). In addition, the aggregated Aβ morphotype, which had a blueshifted HS-68 spectra with a prominent emission at $\lambda =$ 485 nm, was only present in older mice.

In brain tissue from P301S tau mice, HS-68 staining also revealed aggregates with distinct morphologies and different emission profiles. In mice sacrificed at two months, the assemblies were loosely packed, often granular in appearance, and displayed a yellow-red color after HS-68 staining (Figure 2A). This type of aggregate was observed already in one-month-old mice, but in very low numbers. In older mice, a second type of aggregate emerged, which had a dense and homogenously stained morphology. Labeling of these structures with HS-68 resulted in a green color, whereas coexisting aggregates of the first type, which were much fewer in number, continued to emit redshifted light (Figure 2A). As demonstrated by colocalization with the AT8 antibody, both types of morphologies were composed of hyperphosphorylated tau (Figure 2B). Representative emission spectra of HS-68 binding to tau assemblies in mice sacrificed at two, four, or six months confirmed the age-dependent spectral variation (Figure 2C; Supporting Information, Figure S1). Pronounced peaks or shoulders were seen at $\lambda = 485$, 520, 529, and 573 nm to varying degrees. The disappearance of the distinct shoulder at $\lambda = 573$ nm and the appearance of the peak at $\lambda = 485$ nm confirmed that the HS-68 emission profile obtained from aggregated tau morphotypes in older mice was blueshifted. The ratio of the emission intensity at $\lambda = 485$ and 573 nm for HS-68 positive tau aggregates also demonstrated an increased value for older mice (Figure 2C). The marked difference in the ratio between the three- and four-month-old mice indicated that the blueshifted homogenous aggregated tau morphotypes emerged in this period.

From a biological perspective, the transitions of HS-68 emission profiles for both Aβ and tau aggregates could be assigned to a distinct age of the mice. For the APPPS1 mouse model it has previously been shown that the formation of new Aβ deposits is most prominent in young mice, whereas from approximately eight months of age the formation of new deposits was drastically reduced and mostly existing plaques appeared to grow.[32] In addition, the combination of two LCOs, tetramer formyl thiophene acetic acid (q-FTAA) and heptamer formyl thiophene acetic acid (h-FTAA), with separate emission profiles was recently employed to study the age-dependent conformational rearrangement of Aβ deposits.[25] Our results show that the blueshift of HS-68 becomes substantial around the age at which mature amyloid species were detected by q-FTAA.[25] Thus, the spectral transition of HS-68 when interacting with distinct Aβ deposits appears to reflect age-dependent conformational rearrangement within the Aβ aggregates. For P301S tau aggregates, the change in the HS-68 emission profiles as the mice aged was even more evident, and the effect appeared to be caused by the formation of two types of aggregates. A variation of the aggregate type was also described in the original report for this mouse model, in which antibody labeling of tau in five- or six-month-old mice was defined as either homogenous or granular with the appearance of circumscribed inclusions.[30] Herein, HS-68 staining revealed that homogenous aggregates emerged at four months of age, whereas the granular- or inclusion-like structures could be seen already in one-month old mice. Interestingly, the P301S tau mice developed severe disease symptoms at five-to-six months of age, suggesting that the homogenous aggregate type with a blueshifted HS-68 emission profile might be associated with the observed neurodegeneration.[30]

Optical properties of HS-68 in different buffer solution

To elucidate the observed spectral transitions of HS-68 upon interaction with Aβ- or tau aggregates, we next evaluated the conformationally induced photophysical properties of HS-68. It has previously been reported that changes in solvent conditions can alter the optical behavior of LCPs[33] and LCOs,[34] therefore absorption-, emission-, and excitation spectra were recorded for HS-68 in different buffer solutions ranging from pH 3.5 to pH 7 (Figure 3; Supporting Information, Figure S2A). The absorption maximum was blueshifted from $\lambda = 400$ (pH 7) to 379 nm (pH 3.5), which indicated a planar-to-nonplanar transition of the thiophene backbone[35,36] with decreasing pH. In addition, lowering the pH also induced an additional shoulder around $\lambda = 450$ nm in the spectrum (Figure 3A), which was previously assigned to π–π stacking of adjacent thiophene chains.[37]

Excitation of HS-68 at $\lambda = 375$ nm, a wavelength that corresponded to the observed absorption maximum at acidic pH, resulted in a shift of the main emission peak from $\lambda = 510$ to 476 nm on going from neutral to acidic pH (Figure 3B, left). In contrast, when an excitation wavelength equivalent to the observed shoulder in the absorption spectrum ($\lambda = 450$ nm) was used, the emission peak was gradually redshifted from $\lambda = 510$

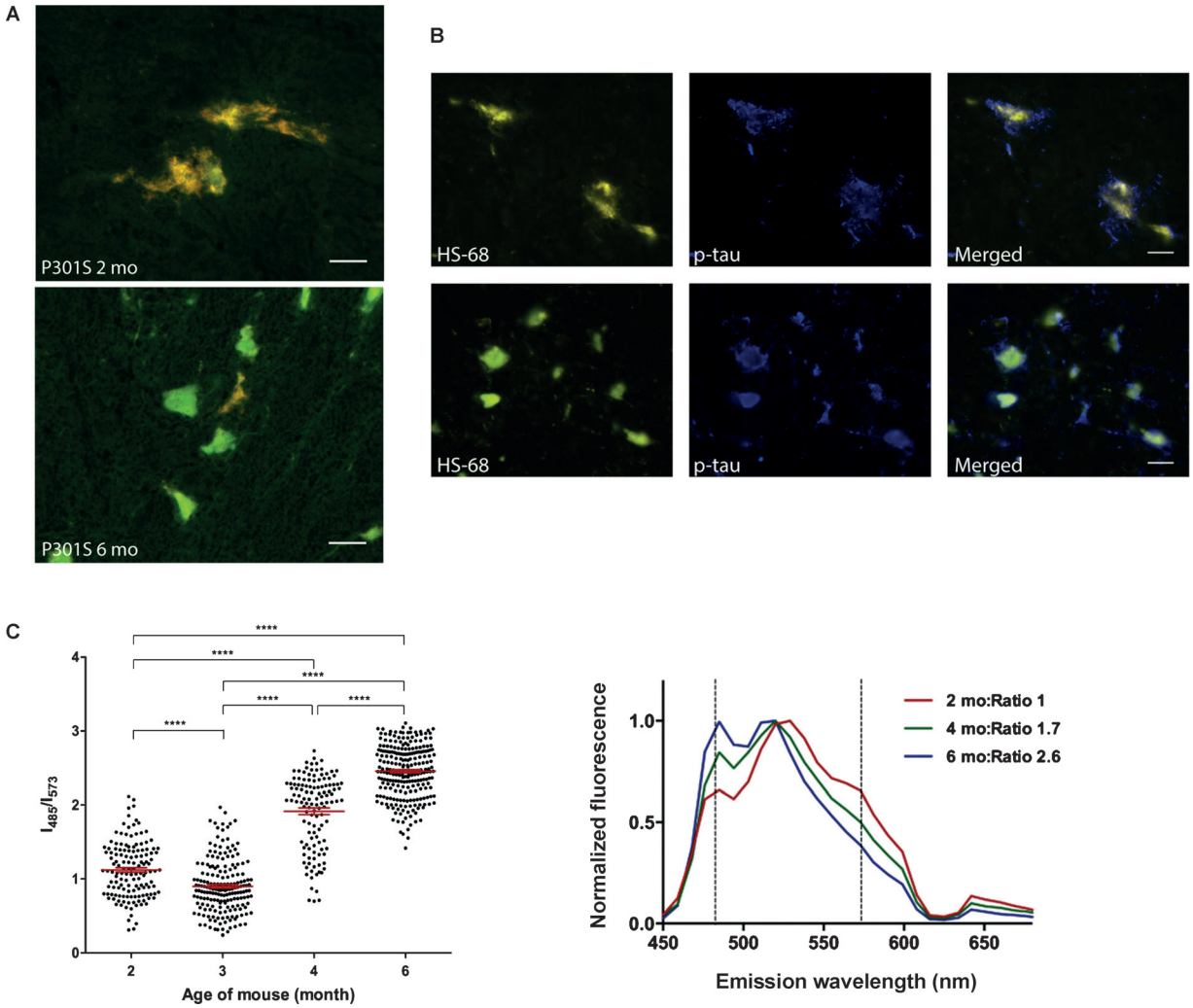

Figure 2. Fluorescence images and emission signal analysis of HS-68 when binding to tau aggregates. A) Fluorescence images of tau aggregates in frozen brain sections from homozygous P301S tau mice stained with HS-68. The mice were sacrificed aged two- or six months and the brain sections were fixed with ethanol before staining with HS-68 (3 μM) in phosphate-buffered saline (pH 7.4). HS-68 labeling revealed two types of aggregates; an early-formed aggregate with redshifted fluorescence (top) and a later-formed aggregate with blueshifted fluorescence (bottom). Scale bars = 20 μm. B) Fluorescence images of tau aggregates in two- (top) or six-month-old (bottom) P301S mice co-stained with HS-68 and AT8 tau antibody. The frozen brain sections were fixed with acetone before staining. Colabeling of the antibody and HS-68 confirmed that both types of HS-68 positive aggregates were composed of tau. Scale bars = 20 μm. c) Plot of the ratio of the fluorescence intensity at $\lambda = 485$ and 573 nm in HS-68 emission spectra (excited at $\lambda = 405$ nm) when binding to tau aggregates in ethanol-fixed frozen brain sections from P301S mice. The group mean and standard error of the mean are indicated. Statistical analysis was performed by one-way analysis of variance followed by Tukey's multicomparison post hoc test. **** = $p < 0.0001$. The spectral graph illustrates representative emission spectra of HS-68 bound to aggregated tau in P301S mice sacrificed aged two-, four-, or six months. Dashed lines (-----) indicate the wavelengths selected to generate the ratio plot.

(pH 7) to 570 nm (pH 3.5) (Figure 3 B, right). Thus, by changing the pH and thereby the charge of the acetic acid ($pK_a = 4.4$) and carboxylic acid ($pK_a = 3.5$) substituents, the emission peaks observed for HS-68 bound to Aβ- or tau aggregates could be largely mimicked. Emission maxima corresponding to the emission peaks at $\lambda = 511$ (Aβ aggregates) and 520 nm (tau aggregates) were obtained for HS-68 with deprotonated side chains (pH 7.0), whereas the additional emission peaks at $\lambda = 485$ and 573 nm, observed from HS-68 bound to different aggregated morphotypes of Aβ and tau, were obtained when the anionic side chains were mostly protonated (pH 3.5). These emission maxima could also be assigned to specific excitation profiles of the dye (Supporting Information, Figure S2 A), which verified that the emission at these wavelengths was related to specific optical transitions induced by conformational alterations of the conjugated thiophene backbone or π–π stacking arrangements between adjacent thiophene chains.

Overall, the photophysical characterization of HS-68 verified that alteration of the charge of the anionic side chains induced distinct backbone conformations and π–π stacking between adjacent thiophene chains. In addition, the predominant emission peaks observed from HS-68 bound to the aggregated Aβ- or tau morphotypes in tissue sections could be recreated in solution. The HS-68 emission peaks at $\lambda = 485$ and 573 nm, associated with the dominating aggregated species in old and young mice, respectively, could be obtained by protonation of

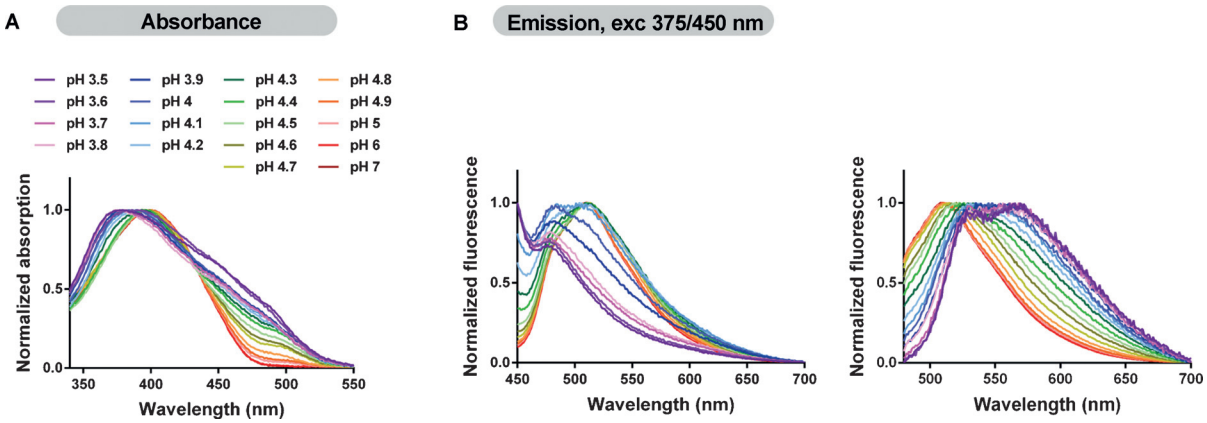

Figure 3. The pH effect on HS-68 photophysical properties. A) Absorbance spectra of HS-68 (30 μM dilution) in buffer (pH values indicated). The blueshifted absorbance and the emergence of a redshifted shoulder at low pH values indicate the formation of distinct types of HS-68 assemblies. B) Emission spectra of HS-68 (30 μM dilution) in buffer (pH values shown in part A). By exciting the probe at $\lambda = 375$ (left) or 450 nm (right) the emission spectra at low pH values were dominated by either blue- or redshifted HS-68 assemblies with peaks corresponding well to the those obtained for HS-68 bound to early- or late-formed Aβ- or tau aggregates.

the anionic side chains. Thus, the intra- and intermolecular interactions occurring along the thiophene backbone or between adjacent thiophene chains at acidic pH, rendered photophysical transitions similar to those obtained from the dye bound to the age-related aggregated species and the two emission peaks at $\lambda = 485$ and 573 nm were also assigned to distinct conformational transitions of the conjugated thiophene backbone or π–π stacking between adjacent thiophene chains. The molecular interactions between HS-68 molecules in solution are most likely different to the molecular interplay between HS-68 and the protein aggregates. However, the optical characterization of HS-68 suggested that the molecular interplay between anionic groups of adjacent thiophene chains influenced the conformationally induced optical properties of the dye, which indicates that electrostatic interactions between the carboxyl groups of HS-68 and positively charged amino acids of the protein aggregates might induce similar optical transitions of the conjugated thiophene backbone.

Synthesis and optical characterization of HS-68 analogues

To further investigate the correlation between the anionic substituents and the optical behavior of the tetrameric thiophene backbone, four chemically related analogues of HS-68 were synthesized (Figure 4A). Relocating the sodium acetate substituent of the second thiophene ring to the other β position or replacing the terminal carboxylate groups with sodium acetate moieties resulted in HS-145 and HS-149, respectively. Adding sodium acetate substituents to positions three or four of the third thiophene unit resulted in HS-129 and HS-136, respectively. The new LCOs were synthesized in a similar fashion to previously reported LCOs (Supporting Information, Schemes S1–S3).[26,28,29,34] After synthesis and purification, the pH-dependent optical changes of the dyes were assessed as described above.

At pH 7, HS-129, HS-145, and HS-149 displayed a similar absorption maximum ($\lambda \approx 400$ nm) to HS-68 (Figure 4B). For HS-136, the absorption maximum was blueshifted to $\lambda = 375$ nm, which indicated that HS-136 adopts a less-planar conformation than the other LCOs. In addition, HS-136 lacked the pH-induced shift of the absorption maximum, whereas HS-145 and HS-149 demonstrated a similar pH-dependent blueshift of the absorption maximum, as well as an additional shoulder in the spectrum ($\lambda \approx 450$ nm), both changes that were noted for HS-68. However, the shoulder at longer wavelengths was less pronounced for HS-149. In contrast to the other HS-68 analogues, HS-129 showed a redshifted absorption maximum with decreasing pH (Figure 4B).

In emission mode, only HS-145 (Figure 4C; Supporting Information, Figure S3) displayed spectral transitions that resembled the fluorescent properties of HS-68 (Figure 3). Excitation of HS-145 at $\lambda = 375$ nm showed a pH-dependent blueshift of the emission maximum at $\lambda = 510$ nm (pH 7) to $\lambda = 482$ nm (pH 3.5), similar to the behavior of HS-68. In addition, excitation of HS-145 at $\lambda = 450$ nm displayed a pronounced pH-dependent redshift of the peak at $\lambda = 510$ nm (pH 7) to $\lambda = 571$ nm (pH 3.5). HS-149 showed the same emission maximum ($\lambda = 497$ nm) for both excitation wavelengths and all tested pH values (Figure 4C). At pH 3.5, minor shoulders at shorter or longer wavelengths were also observed, depending on the excitation wavelength. Similarly to HS-68 and HS-145, HS-129 demonstrated a pH-dependent redshift of the emission maximum at $\lambda = 512$ nm (pH 7) to $\lambda = 560$ nm (pH 3.5) when excited at $\lambda = 450$ nm (Figure 4C). However, excitation at $\lambda = 375$ nm also yielded a redshifted emission maximum. HS-136 only displayed a minor pH-dependent redshift of the emission maximum when excited at $\lambda = 450$ nm (Figure 4C). Recording the excitation maximum with the emission fixed at the respective maxima ($\lambda = 510$ or 575 nm) also confirmed that HS-145 was the only analogue to display similar transitions to HS-68 (Supporting Information, Figure S2). Overall, the results obtained from the optical characterization of the HS-68 analogues verified that minor alterations of the spacing between the anionic groups along the tetrameric thiophene backbone highly influenced the pH-dependent optical characteristics of the dyes.

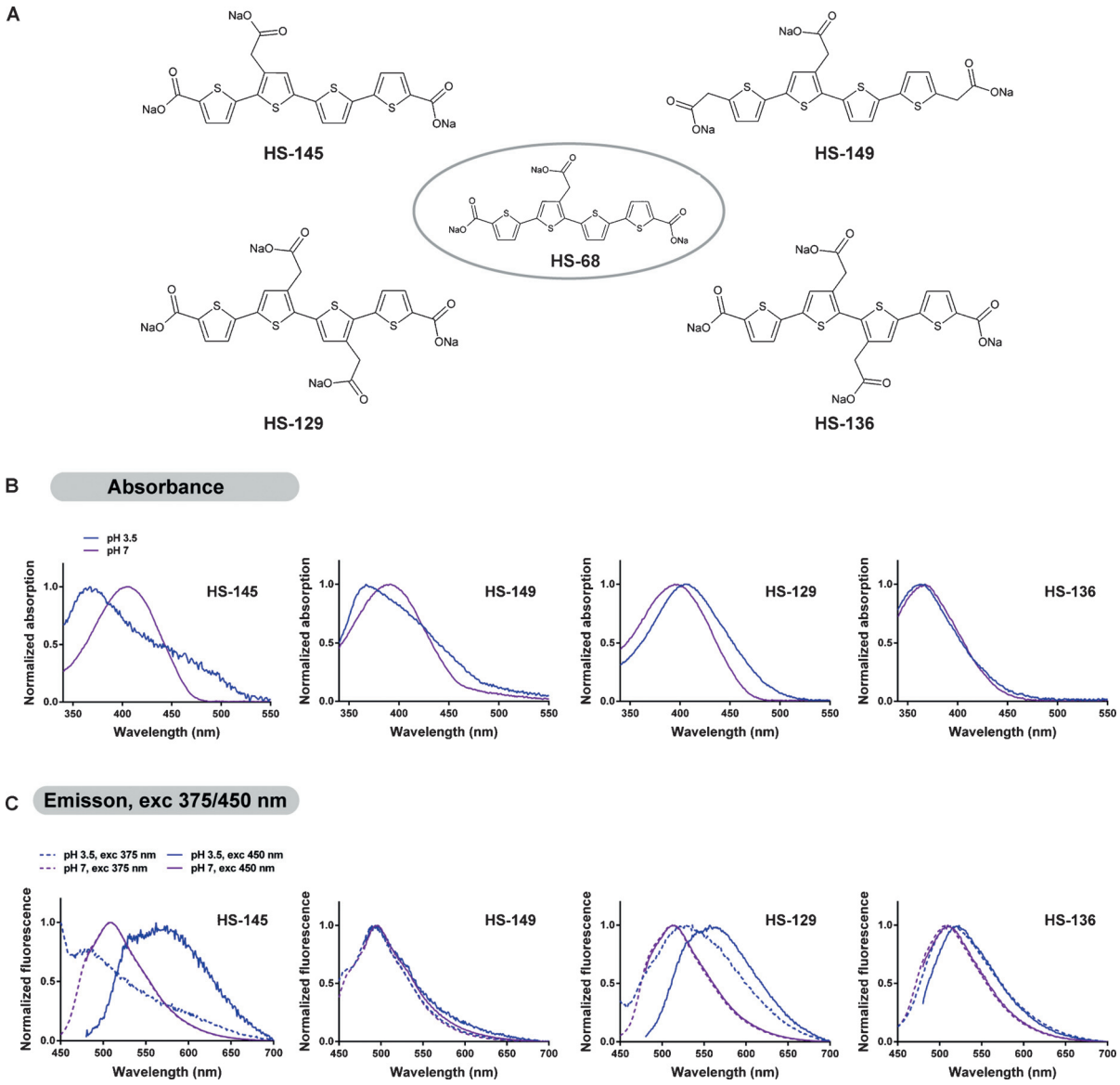

Figure 4. Chemical structures and pH-dependent photophysical properties of HS-68 analogues. A) The sodium salt of HS-68 and its analogues HS-145, HS-149, HS-129, and HS-136. B) Absorbance spectra of the HS-68 analogues (30 μM dilution) in pH 3.5 (blue) or pH 7 (magenta) buffer. The pH effect on HS-145 absorbance properties is similar to what was observed with HS-68, which indicates that this structure also forms distinct types of assemblies at pH 3.5. An analogous pattern of pH-induced wavelength shifts is seen with HS-149, but not as pronounced as with HS-68 and HS-145. The absorbance properties of HS-136 appear to be pH independent, whereas its structural analogue HS-129 displays a spectral redshift with decreasing pH. C) Emission spectra of the HS-68 analogues (30 μM dilution) in pH 3.5 (blue) or pH 7 buffer (magenta), excited at $\lambda = 375$ (-----) or 450 nm (——). By choosing the optimal excitation wavelength it is possible to distinguish blue- and redshifted HS-145 assemblies at pH 3.5, similar to the observations with HS-68, whereas the photophysical properties of HS-149 seem to be pH independent. The emission spectra of HS-129 and, to some extent HS-136, indicate the formation of redshifted assemblies at low pH, but none of the probes demonstrate any blueshift.

HS-68 analogues for spectral assignment of aggregated morphotypes

The distance between the carboxyl groups along the tetrameric thiophene backbone influenced the pH-induced optical properties of the tetrameric LCOs, therefore we next investigated the emission spectra of HS-68 analogues bound to morphotypes of Aβ- or tau aggregates in tissue sections. As reference samples, sections from one young (148 d) and one old (531 d) APPPS1 mouse, as well as three young (two to three months) and three old (six months) P301S tau mice were selected. The statistical analysis of the HS-68 emission profiles when bound to the Aβ- and tau aggregates in these references samples are shown in Table 1. It was evident from the differences in the group mean values that HS-68 could be utilized for spectral separation of age-related aggregated Aβ- and tau morphotypes in these samples.

All HS-68 analogues demonstrated specific binding to immunopositive Aβ aggregates (Figure 5). The response of HS-145 and HS-149 closely resembled that of HS-68 and showed strong staining of the central parts of the deposits, as well as the surrounding diffuse amyloid (Figure 5 A, B). In contrast, for

Table 1. Statistical analysis[a] of the spectral difference between aggregated Aβ and tau morphotypes.

LCO[b]	Aβ		Tau	
	Difference of the mean	R^2	Difference of the mean	R^2
HS-68	-0.6330 ± 0.0126	0.9207	-1.0060 ± 0.0530	0.5842
HS-145	-0.0437 ± 0.0130	0.0640	0.0204 ± 0.0147	0.0068
HS-149	-0.2674 ± 0.0420	0.1899	0.3403 ± 0.0289	0.3371
HS-129	-0.3810 ± 0.0194	0.7466	N.D.[c]	N.D.
HS-136	0.0272 ± 0.0043	0.2695	0.0977 ± 0.0133	0.2331

[a] Unpaired t-test with Welch's correction. [b] For structures see Figure 4A. [c] Not determined.

the majority of plaques, HS-129 and HS-136 only labeled the compact cores (Figure 5C,D). In the old P301S tau mice, all probes labeled the aggregates and showed colocalization with the AT8 tau antibody (Figure 5). However, staining with HS-129 and HS-136 was weak, and in the two-month-old mice it was very difficult to detect any HS-129 positive tau aggregates, which made it impossible to collect spectra for analysis (Figure 5C, Table 1).

When binding to aggregated Aβ or tau in the old mice, the emission of HS-145 occurred at similar wavelengths to the emission of HS-68, but the age-dependent transitions of the spectrum were almost abolished (Supporting Information, Figure S4A). When analyzing the fluorescence intensity ratio at $\lambda = 485$ and 564 nm for Aβ aggregates stained with HS-145, the difference between the mean values for the young and old APPS1 mice was considerably reduced compared to HS-68, although still significantly different (Figure 5A, Table 1). In addition, the R^2 value from the unpaired t-test was 0.064 for HS-145, which meant that only 6% of all the variation among the obtained values could be ascribed to differences between the mean values of the two groups. Statistical analysis of tau aggregates stained with HS-145 in the young and old P301S mice showed that the two groups were not significantly different (Figure 5A, Table 1). HS-149 demonstrated a significant spectral difference between the Aβ aggregates in the young and old APPPS1 mice (Figure 5B, Table 1). Similar to the results obtained for HS-68, a pronounced shoulder around $\lambda = 570$ nm was observed in the emission from HS-149 when bound to Aβ aggregates in the young APPPS1 mouse (Supporting Information, Figure S4B). However, the difference between the mean values, as well as the R^2 value, for the two cohorts of aggregates was lower than for HS-68 (Figure 5B, Table 1). A significant difference was also observed for the two groups of tau aggregates stained with HS-149 (Table 1) but, in contrast to HS-68, the tau aggregates in the older mice displayed more-redshifted spectra compared with the spectra obtained from tau deposits in the younger mice (Supporting Information, Figure S4B).

The additional sodium acetate substitution along the thiophene backbone in HS-129 and HS-136 also influenced the emission profiles when bound to aggregated Aβ- and tau morphotypes. It was impossible to collect reliable spectra from tau aggregates in the young mice, hence a comparison between the age-related tau morphotypes could not be assessed by HS-129. However, when analyzing the emission profiles from HS-129 bound to the age-related Aβ morphotypes it was evident that HS-129 could be utilized, to some extent, to distinguish between these aggregated species (Figure 5C and Table 1). Similar to HS-68, the emission profile of HS-129 was redshifted for the old-mice samples, but the difference between the mean values of the samples was not as striking as for HS-68. The emission spectra of HS-136 was very well resolved and extremely blueshifted compared to the other LCOs (Supporting Information, Figure S4D). In addition, with HS-136 the difference between the mean values for both the Aβ- and tau aggregated morphotypes was greatly reduced relative to the values obtained with HS-68 (Figure 5D, Table 1). All the LCOs were also tested for tissue sections from an additional pair of APPS1 mice (245 and 457 d) and the statistical analysis of the spectral difference between the aggregated Aβ morphotypes resembled the results obtained from the first pair of mice (Supporting Information, Table S1).

Taken together, the results from the spectral characterization of the HS-68 analogues bound to the age-related aggregated morphotypes of Aβ and tau clearly showed that the chemical design of the tetrameric LCO greatly influenced the dye's performance as a fluorescent amyloid ligand. First, relocating the sodium acetate moiety on the second thiophene ring from position three to four, generated LCO HS-145, which had a greatly reduced ability to distinguish Aβ- or tau morphotypes. Remarkably, HS-145 displayed pH-dependent optical transitions that were almost identical to those of HS-68, which confirmed that HS-145 can adopt conformational states that render emission at $\lambda = 485$ or 573 nm. However, the pronounced redshifted emission was not observed from the dye bound to the Aβ- or tau morphotypes present in young mice. Thus, moving the sodium acetate group by just one position abolished the conformational rearrangement of the thiophene backbone observed for HS-68 when bound to these aggregated morphotypes, which confirmed that the anionic substituents must be positioned in a chemically defined fashion to achieve sensitive spectral separation. Second, replacing the terminal carboxyl groups on the thiophene backbone with sodium acetate moieties also reduced the spectral separation of both aggregated morphotypes. This implied that having terminal carboxyl groups at an exact distance relative to the central sodium acetate side chain is also essential to achieve a tetrameric LCO that can spectrally distinguish Aβ- and tau morphotypes. Third, addition of a sodium acetate substituent on the third thiophene ring of the HS-68 scaffold diminished the spectral separation of the aggregated morphotypes, and weakened the staining of some aggregated species. Furthermore, the dramatic blueshift observed for HS-136 bound to the deposits indicates a more twisted and rigid conformation of this dye than of the other LCOs. HS-136 also demonstrated less spectral variation for the Aβ morphotypes than observed with HS-129, which verified that the minor structural difference (the central sodium acetate moieties in a head-to-head (HS-136) or head-to-tail (HS-129) configuration) was reflected in the emission profiles from these dyes bound to the aggregated species. Al-

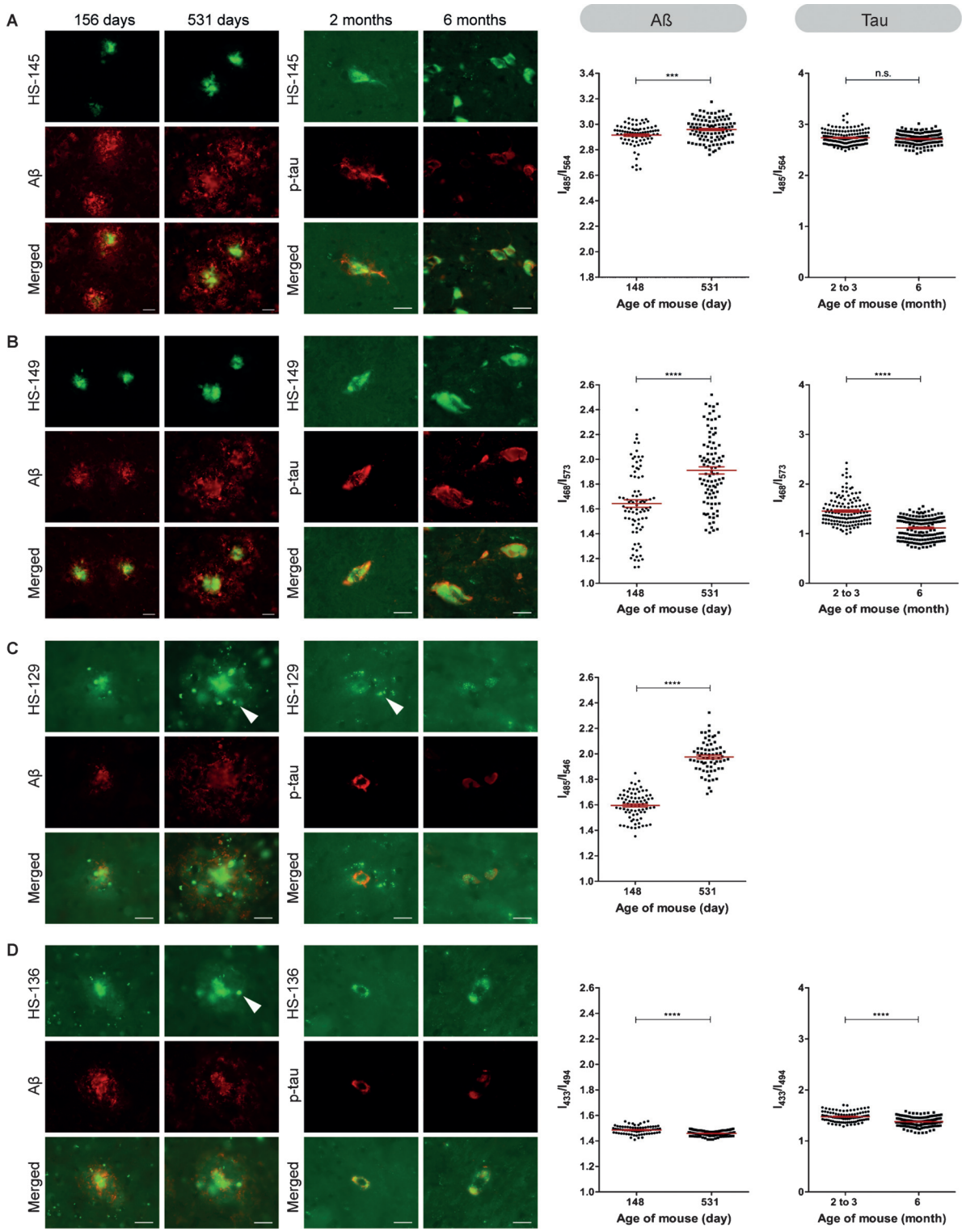

Figure 5. Spectral analyses and fluorescence images of HS-68 analogues bound to Aβ- deposits and aggregated tau. Frozen brain sections from APPPS1 or P301S tau mice sacrificed at the indicated ages were fixed with acetone for LCO and Aβ/phosphorylated tau (p-tau) antibody double-staining experiments (left) and with ethanol for LCO spectral evaluation (right). The ratio plots are calculated from the emission intensity at the specified wavelengths for each LCO when binding to Aβ or tau. The mean and standard error of the mean are indicated and statistical analysis was performed by using the unpaired t-test. **** = $p < 0.0001$, *** = $p < 0.005$, n.s. = non-significant. Scale bars = 20 μm. Arrowheads indicate auto-fluorescence. A) HS-145 shows high-intensity labeling of the aggregates, similar to HS-68, but is the least-efficient probe for achieving age-related spectral separation of Aβ and tau. B) HS-149 labeling of Aβ and tau is strong. The emission signatures vary and the age-dependent spectral difference is pronounced, but with opposite shifts compared to HS-68. C) HS-129 shows weak labeling of Aβ- and tau aggregates, particularly in young P301S tau mice, which prevented spectral analysis. The probe displays a relatively large variation in Aβ spectral signatures and the difference between young and old mice is significant, although not as pronounced as with HS-68. D) HS-136 labeling is weak, but can be used to detect Aβ- or tau aggregates in both young and old animals. It shows less spectral separation and an opposite shift compared with HS-68.

together, our results demonstrate a clear structure–activity relationship between the spacing of anionic substituents along the thiophene backbone and the capacity of the ligand to distinguish aggregated Aβ- and tau morphotypes.

The list of proteins and peptides reported to form different types, or strains, of aggregates is growing, and studies on patient material have indicated that the variation of aggregated morphotypes might explain the heterogeneity of AD and PD phenotypes.[12,17] As a consequence, it has been suggested that therapeutic agents need to be tailored for each patient to combat the specific strain type, and the development of sensitive methods for detection and characterization of distinct aggregate morphotypes is essential. Hence, our finding that the spacing of anionic side chains along the thiophene backbone is an essential chemical determinant for achieving thiophene-based ligands that distinguish polymorphic aggregates of Aβ or tau is of great interest because the majority of amyloid ligands are based on hydrophobic molecular scaffolds that lack charged substituents.[4] Conventional amyloid ligands are mainly utilized for the assessment of protein aggregates in general; however, the introduction and optimization of novel molecular scaffolds has resulted in probes that can distinguish between Aβ- and tau aggregates, the two major pathological hallmarks of AD.[26–29,38,39] Recent studies[26,28,29] have shown that distinct positioning of anionic charges along the conjugated thiophene backbone is a crucial factor to obtain LCOs that can be utilized for the spectral separation of protein deposits comprised of different proteins. In addition, it has been shown that the birefringent properties of Congo red bound to HET-S prion fibrils can be altered by disrupting the interactions between the two sulfonate groups in Congo red and the positively charged side chains on the surface of the fibril.[40] Thus, electrostatic interactions between the ligand and the fibrils are essential determinants for the optical performance of amyloid ligands. From a chemical perspective, the design of ligands with a distinct arrangement of chemical groups that form complementary electrostatic interactions with the protein aggregates might be crucial to obtain ligands for distinct aggregated morphotypes.

Conclusion

The tetrameric LCO HS-68 was identified as an optical ligand for revealing age-dependent polymorphism of Aβ- or tau aggregates. The superior functionality of the dye compared with structurally related compounds was assigned to distinct spacing between the anionic groups along the conjugated backbone. We foresee that our findings will aid the chemical design of ligands that could be utilized for exploring aggregated morphotypes that might underlie the heterogenic phenotypes observed for neurodegenerative protein-aggregation disorders. Such ligands will also be vital for evaluating novel therapeutic strategies for these diseases.

Experimental Section

Full experimental details, including additional characterization data and NMR spectra of new compounds are given in the Supporting Information. All animal experiments were performed in accordance with the UK Animal (Scientific Procedures) Act 1986 for the welfare of laboratory animals (United Kingdom) or the veterinary office regulations of Baden-Württemberg (Germany) and were approved by the Medical Research Council local animal welfare and ethical review board (United Kingdom) or the local Animal Care and Use Committees (Germany).

Acknowledgements

Our work is supported by the Swedish Foundation for Strategic Research (K.P.R.N., T.K.) and the Swedish Alzheimer Foundation (S.N.). K.P.R.N. is financed by an European Research Council Starting Independent Researcher Grant (Project: MUMID). The authors would like to thank Isabelle Lavenir for technical support.

Keywords: aggregates · Alzheimer's disease · fluorescence · luminescent conjugated oligothiophenes · proteins

[1] F. Chiti, C. Dobson, *Ann. Rev. Biochem.* **2006**, *75*, 333–366.
[2] E. D. Eanes, G. G. Glenner, *J. Histochem. Cytochem.* **1968**, *16*, 673–677.
[3] L. Bonar, A. S. Cohen, M. M. Skinner, *Proc. Soc. Exp. Biol. Med.* **1969**, *131*, 1373–1375.
[4] K. P. R. Nilsson, *FEBS Lett.* **2009**, *583*, 2593–2599.
[5] W. E. Klunk, B. J. Bacskai, C. A. Mathis, S. T. Kajdasz, M. E. McLellan, M. P. Frosch, M. L. Debnath, D. P. Holt, Y. Wang, B. T. Hyman, *J. Neuropathol. Exp. Neurol.* **2002**, *61*, 797–805.
[6] W. E. Klunk, H. Engler, A. Nordberg, Y. Wang, G. Blomqvist, D. P. Holt, M. Bergström, I. Savitcheva, G. F Huang, S. Estrada, B. Ausén, M. L. Debnath, J. Barletta, J. C. Price, J. Sandell, B. J. Lopresti, A. Wall, P. Koivisto, G. Antoni, C. A. Mathis, B. Långström, *Ann. Neurol.* **2004**, *55*, 306–319.
[7] H. Levine, L. C. Walker, *Neurobiol. Aging* **2010**, *31*, 542–548.
[8] B. H. Toyama, J. S. Weissman, *Ann. Rev. Biochem.* **2011**, *80*, 557–585.
[9] D. Eisenberg, M. Jucker, *Cell* **2012**, *148*, 1188–1203.
[10] L. Bousset, L. Pieri, G. Ruiz-Arlandis, J. Gath, P. H. Jensen, B. Habenstein, K. Madiona, V. Olieric, A. Böckmann, B. H. Meier, R. Melki, *Nat. Commun.* **2013**, *4*, 2575.
[11] F. Clavaguera, H. Akatsu, G. Fraser, R. A. Crowther, S. Frank, J. Hench, A. Probst, D. T. Winkler, J. Reichwald, M. Staufenbiel, B. Ghetti, M. Goedert, M. Tolnay, *Proc. Natl. Acad. Sci. USA* **2013**, *110*, 9535–9540.
[12] J. L. Guo, D. J. Covell, J. P. Daniels, M. Iba, A. Stieber, B. Zhang, D. M. Riddle, L. K. Kwong, Y. Xu, J. Q. Trojanowski, V. M. Lee, *Cell* **2013**, *154*, 103–117.
[13] J. Collinge, A. R. Clarke, *Science* **2007**, *318*, 930–936.
[14] C. L. Maarouf, I. D. Daugs, S. Spina, R. Vidal, T. A. Kokjohn, R. L. Patton, V. L. Kalback, D. C. Luehrs, D. G. Walker, E. M. Castano, T. G. Beach, B. Ghetti, A. B. Roher, *Mol. Neurodegener.* **2008**, *3*, 20.
[15] M. Meyer-Luehmann, J. Coomaraswamy, T. Bolmont, S. Kaeser, C. Schaefer, E. Kilger, A. Neuenschwander, D. Abramowski, P. Frey, A. L. Jaton, J.-M. Vigouret, P. Paganetti, D. M. Walsh, P. M. Mathews, J. Ghiso, M. Staufenbiel, L. C. Walker, M. Jucker, *Science* **2006**, *313*, 1781–1784.
[16] A. T. Petkova, R. D. Leapman, Z. Guo, W. M. Yau, M. P. Mattson, R. Tycho, *Science* **2005**, *307*, 262–265.
[17] J. X. Lu, W. Qiang, W. M. Yau, C. D. Schwieters, S. C. Meredith, R. Tycho, *Cell* **2013**, *154*, 1257–1268.
[18] F. Clavaguera, I. Lavenir, B. Falcon, M. Goedert, M. Tolnay, *Brain Pathol.* **2013**, *23*, 342–349.
[19] T. Klingstedt, K. P. R. Nilsson, *Biochim. Biophys. Acta.* **2011**, *1810*, 286–296.

[20] C. J. Sigurdson, K. P. R. Nilsson, S. Hornemann, G. Manco, M. Polymenidou, P. Schwartz, M. Leclerc, P. Hammarström, K. Wüthrich, A. Aguzzi, *Nat. Meth.* **2007**, *4*, 1023 – 1030.
[21] K. Magnusson, R. Simon, D. Sjölander, C. J. Sigurdson, P. Hammarström, K. P. R. Nilsson, *Prion* **2014**, *8*, 319 – 329.
[22] K. P. R. Nilsson, K. Ikenberg, A. Åslund, S. Fransson, P. Konradsson, C. Röcken, H. Moch, A. Aguzzi, *Am. J. Pathol.* **2010**, *176*, 563 – 574.
[23] K. P. R. Nilsson, A. Åslund, I. Berg, S. Nyström, P. Konradsson, A. Herland, O. Inganäs, F. Stabo-Eeg, M. Lindgren, G. T. Westermark, L. Lannfelt, L. N. Nilsson, P. Hammarström, *ACS Chem. Biol.* **2007**, *2*, 553 – 560.
[24] G. Heilbronner, Y. S. Eisele, F. Langer, S. A. Kaeser, R. Novotny, A. Nagarathinam, A. Åslund, P. Hammarström, K. P. R. Nilsson, M. Jucker, *EMBO Rep.* **2013**, *14*, 1017 – 1022.
[25] S. Nyström, K. M. Psonka-Antonczyk, P. G. Ellingsen, L. B. G. Johansson, N. Reitan, S. Handrick, S. Prokop, F. L. Heppner, B. M. Wegenast-Braun, M. Jucker, M. Lindgren, B. T. Stokke, P. Hammarström, K. P. R. Nilsson, *ACS Chem. Biol.* **2013**, *8*, 1128 – 1133.
[26] A. Åslund, C. J. Sigurdson, T. Klingstedt, S. Grathwohl, T. Bolmont, D. L. Dickstein, E. Glimsdal, S. Prokop, M. Lindgren, P. Konradsson, D. M. Holtzman, P. R. Hof, F. L. Heppner, S. Gandy, M. Jucker, A. Aguzzi, P. Hammarström, K. P. R. Nilsson, *ACS Chem. Biol.* **2009**, *4*, 673 – 684.
[27] B. M. Wegenast-Braun, A. Skodras, G. Bayraktar, J. Mahler, S. K. Fritschi, T. Klingstedt, J. J. Mason, P. Hammarström, K. P. R. Nilsson, C. Liebig, *Am. J. Pathol.* **2012**, *181*, 1953 – 1960.
[28] T. Klingstedt, A. Åslund, R. A. Simon, L. B. G. Johansson, J. J. Mason, S. Nyström, P. Hammarström, K. P. R. Nilsson, *Org. Biomol. Chem.* **2011**, *9*, 8356 – 8370.
[29] T. Klingstedt, H. Shirani, A. Åslund, N. J. Cairns, C. J. Sigurdson, M. Goedert, K. P. R. Nilsson, *Chem. Eur. J.* **2013**, *19*, 10179 – 10192.
[30] B. Allen, E. Ingram, M. J. Takao, R. Jakes, K. Virdee, H. Yoshida, M. Holzer, M. Craxton, P. C. Emson, C. Atzori, A. Migheli, R. A. Crowther, B. Ghetti, M. G. Spillantini, M. Goedert, *J. Neurosci.* **2002**, *22*, 9340 – 9351.
[31] R. Radde, T. Bolmont, S. S. Kaeser, J. Coomaraswamy, D. Lindau, L. Stoltze, M. E. Calhoun, F. Jaggi, H. Wolburg, S. Gengler, C. Haass, B. Ghetti, C. Czech, C. Holscher, P. M. Mathews, M. Jucker, *EMBO Rep.* **2006**, *7*, 940 – 946.
[32] J. K. Hefendehl, B. M. Wegenast-Braun, C. Liebig, D. Eicke, D. Milford, M. E. Calhoun, S. Kohsaka, M. Eichner, M. Jucker, *J. Neurosci.* **2011**, *31*, 624 – 629.
[33] B. Kim, L. Chen, J. Gong, Y. Osada, *Macromolecules* **1999**, *32*, 3964 – 3969.
[34] R. A. Simon, H. Shirani, K. O. Åslund, M. Bäck, V. Haroutunian, S. Gandy, K. P. R. Nilsson, *Chem. Eur. J.* **2014**, *20*, 12537 – 12543.
[35] J. L. Brédas, G. B. Street, B. Thémans, J. M. André, *J. Chem. Phys.* **1985**, *83*, 1323 – 1329.
[36] C. Roux, M. Leclerc, *Macromolecules* **1992**, *25*, 2141 – 2144.
[37] K. Faid, M. Leclerc, *J. Am. Chem. Soc.* **1998**, *120*, 5274- 5278.
[38] A. Taghavi, S. Nasir, M. Pickhardt, R. Heyny-von Haussen, G. Mall, E. Mandelkow, E. M. Mandelkow, B. Schmidt, *J. Alzheimers Dis.* **2011**, *27*, 835 – 843.
[39] M. Maruyama, H. Shimada, T. Suhara, H. Shinotoh, B. Ji, J. Maeda, M. R. Zhang, J. Q. Trojanowski, V. M. Lee, M. Ono, K. Masamoto, H. Takano, N. Sahara, N. Iwata, N. Okamura, S. Furumoto, Y. Kudo, Q. Chang, T. C. Saido, A. Takashima, J. Lewis, M. K. Jang, I. Aoki, H. Ito, M. Higuchi, *Neuron* **2013**, *79*, 1094 – 1108.
[40] A. K. Schütz, A. Soragni, S. Hornemann, A. Aguzzi, M. Ernst, A. Bockmann, B. H. Meier, *Angew. Chem. Int. Ed. Engl.* **2011**, *50*, 5956 – 5960; *Angew. Chem.* **2011**, *123*, 6078 – 6082.

Received: February 10, 2015
Published online on May 26, 2015

